



PERGAMON

Deep-Sea Research II 49 (2002) 1297–1322

DEEP-SEA RESEARCH
PART II

www.elsevier.com/locate/dsr2

Abyssal circulation in the Somali Basin

M. Dengler^{a,*}, D. Quadfasel^b, F. Schott^a, J. Fischer^a

^a*Institut für Meereskunde an der Universität Kiel, Düsternbrooker Weg 20, 24105 Kiel, Germany*

^b*Niels Bohr Institutet for Astronomi, Fysik og Geofysik, Københavns Universitet, Juliane Maries Vej 30, 2100 Copenhagen, Denmark*

Accepted 20 September 2001

Abstract

The bottom and deep circulation in the Somali Basin are investigated on the basis of hydrographic and direct velocity profiles from three shipboard surveys carried out during the southwest monsoon in 1995 and of velocity time series from the WOCE mooring array ICM7. The inflow of bottom water into the Somali Basin through the Amirante Passage drives a thermohaline circulation, which may be modulated by the monsoon wind forcing. Details of the abyssal circulation have been discussed controversially. Deep velocity records from the mooring array in the northern Somali Basin are dominated by fluctuations with periods of 30–50 days and amplitudes above 5 cm s^{-1} . Despite this strong variability annual record averages indicate the existence of a deep western boundary current (DWBC) below 3000 m at the base of the continental slope south of Socotra Island as part of a cyclonic bottom circulation. The southwestward DWBC transport off Socotra Island is estimated to $2 \pm 1.3 \text{ Sv}$. The bottom and deep water exchange between the Somali and Arabian Basin north of 7°N is estimated from two cross-basin geostrophic velocity sections referenced by vertically averaged LADCP currents. For the bottom water, an eastward transport into the Arabian Basin of $1.4 \pm 0.5 \text{ Sv}$ and $2.1 \pm 0.6 \text{ Sv}$ was determined in June and August, respectively, while for the deep-water layer above 3500 m eastward transports of $3.6 \pm 2.3 \text{ Sv}$ in June and $4.0 \pm 2.4 \text{ Sv}$ in August were obtained. © 2002 Elsevier Science Ltd. All rights reserved.

1. Introduction

The Indian Ocean is bounded to the north by land at subtropical latitudes. There is a net buoyancy flux into the Indian Ocean north of 12°S (Zhang and Talley, 1998), inhibiting the formation of deep water. The deep water in the northern abyssal basins is thus supplied from the south.

Dense abyssal waters from Antarctica characterized by low temperatures, low salinities, and high oxygen contents spread northward along the western and eastern margins of the Indian Ocean. The eastern inflow ventilates the Australian and central Indian Basins, while the western branch supplies the Mascarene, Somali and Arabian Basins. Here, Circumpolar Deep Water (CDW) enters the Madagascar Basin through the discordance zones in the Southwestern Indian Ridge (Warren, 1978). As a deep western boundary current (DWBC), it flows northward into the Mascarene Basin and enters the Somali Basin via the 4600 m deep Amirante Passage (Fig. 1).

*Corresponding author. Tel.: +49-431-600-4107; fax: +49-431-600-4102.

E-mail address: mdengler@ifm.uni-kiel.de (M. Dengler).

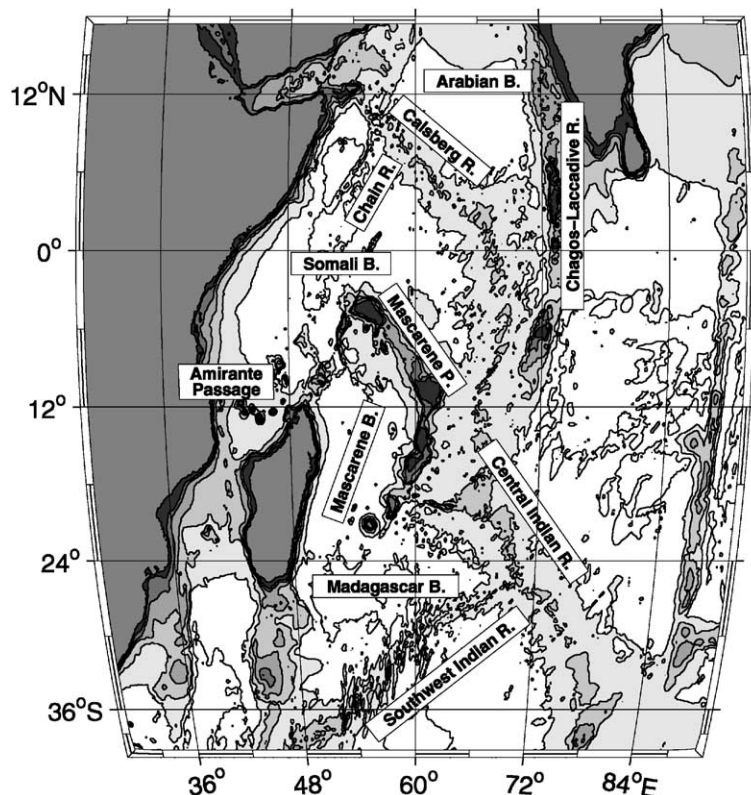


Fig. 1. Bathymetric features and names in the western Indian Ocean (B. is basin, R. is ridge P. is plateau). Filled contours are 4000 m (light gray), 3000, 2000, 1000 and 200 m depths.

The first direct evidence of rapid northward bottom flow through the Amirante Passage came from an analysis of the microtopography and regional sediment distribution based on continuous seismic-reflection profiles and echograms (Johnson and Damuth, 1979). The northward transport of CDW through the passage is now fairly well established. On the basis of three WOCE sections and three pre-WOCE sections Johnson et al. (1998) estimated an inflow into the Somali Basin of 1.0–1.7 Sv ($1 \text{ Sv} = 1 \times 10^6 \text{ m}^3 \text{ s}^{-1}$) below 4000 m depth, in agreement with previous estimates by Fioux and Swallow (1988).

The Somali Basin is bounded to the south by the Mascarene Plateau and the Central Indian Ridge, to the west by the African continent and to the east by the Carlsberg Ridge (Fig. 1). The Owen fracture zone, a gap in the Carlsberg Ridge near 11°N , 57°E , with a depth of 3800 m (Wyrтки, 1971)

connects the Somali Basin with the Arabian Basin. Bottom water from the Somali Basin crosses this sill and ventilates the deep Arabian Basin. The average transport of the throughflow below 3000 m depth was estimated to about 2 Sv, with a seasonal modulation of the same magnitude (Johnson et al., 1991b; Quadfasel et al., 1997). The CDW entering through the Amirante Passage below 3800 m thus has to upwell in the Somali Basin to continue its path into the Arabian Basin. A passage at depth 3500–4000 m also exists at the southeastern tip of the Arabian Basin near 6°S in the Chagos-Laccadive ridge (Fig. 1), connecting the Arabian Basin to the Central Indian Basin (Fischer et al., 1982). To date, an exchange of deep water through this passage has not been documented.

Above the bottom water, deep water characterized by high salinities, high-silicate and

low-oxygen contents is found in the depth range between about 2000 and 3500 m (Warren, 1993). This water mass is often referred to as the Indian Ocean Deep Water (IDW) (e.g., Warren and Johnson, 1992; Toole and Warren, 1993). IDW is composed of upwelled CDW and water masses from intermediate depths in the Arabian Sea and perhaps the Bay of Bengal (e.g., Warren and Johnson, 1992; Warren, 1993).

A southward movement of IDW south of the equator at subtropical latitudes has been observed by several authors (e.g., Warren, 1981b; Spencer et al., 1982; Toole and Warren, 1993). Results from a recent global inverse model suggest 7 ± 3 Sv of IDW to flow southward across 18°S (Sloyan and Rintoul, 2001). In the Amirante passage, Johnson et al. (1998) found IDW flowing southward above the northward-flowing CDW. The estimated transport resulted in 4–8 Sv, much larger than the inflow into the Somali Basin. Given that IDW is transformed CDW returning south, the authors suggested a westward flow of upwelled CDW in the deep eastern basins of the Indian Ocean north of the Amirante Passage in depths unconstrained by topography.

To account for the different abyssal water mass characteristics and their induced circulation schemes, we will follow Warren and Johnson (1992) by using “bottom water” to describe the layer below 3500 m depths and “deep water” for the layer between 2000 and 3500 m depths throughout this paper. “Abyssal” refers to both deep and bottom layer.

The abyssal circulation in the Somali Basin itself has been discussed controversially. The first inferences of a circulation pattern were made by Warren et al. (1966). Maps of salinity on potential temperature surfaces from 130 Nansen bottle stations collected during the southwest monsoon period in August and September 1964 revealed a band of fresh deep water along the continental slope of Somalia. An eastward extension of this band was found at about 10°N . Warren et al. (1966) interpreted this feature as a deep western boundary current crossing the equator and leading to an anticyclonic circulation pattern in the northern Somali Basin.

On the contrary, geostrophic calculations based on data from April 1984 by Fieux et al. (1986) suggested a cyclonic abyssal circulation. They determined a southward deep boundary current at the continental slope of Somalia north of the equator with velocities of up to 22 cm s^{-1} and a westward transport of 3.6 Sv at the base of the northern continental slope south of Socotra Island between 2000 and 5000 m depths. In the deep-water layer, higher salinities were found farther to the south at the western boundary than in the interior of the northern part of the basin. No clear pattern was identifiable in the bottom water.

A possible linkage of the deep circulation to the monsoon was suggested by Schott et al. (1989) based on a current meter record from the equator at a depth of 3000 m during 1985/86. The currents showed strong seasonality parallel to the coast in phase with the surface current with northeastward mean flow of 10 cm s^{-1} during June to September and 7 cm s^{-1} southwestward flow during November to February. Records at intermediate depths showed little (1000 and 1500 m) or no (2000 m) seasonality. The distribution of salinity in the deep water in October 1986 was comparable to the observations from Fieux et al. (1986) in 1984.

Two repeat CTD sections at the height of subsequent monsoon periods in the Somali Basin at 4°S , on the equator and at about 8°N showed only small seasonal differences in the geostrophic circulation of the bottom water (Johnson et al., 1991a). At 4°S the shoaling of the water property isopleths towards the continental slope suggested the presence of a DWBC. Geostrophic estimates below about 3800 m yielded a northward CDW transport of 3.9 Sv during January 1987 and 4.6 Sv in the same direction during July 1987. Due to lack of guidance from the tracer field, no geostrophic transports were computed for the northern sections. Yet, geostrophic shears within 1° of the equator suggested that the bottom water turns eastward there. The presence of a large mass of cold water in the interior of the basin east of the Chain Ridge (Fig. 1) further suggested an eastward flow at the equator, with some water branching northward into the interior of the northern Somali Basin.

Johnson et al. (1991a) showed the observed bottom circulation to be consistent with the dynamical framework of the deep-mean circulation by Stommel and Arons (1960). Under the assumptions of a flat bottom basin of 4000 m depth with realistic geometry and uniform upwelling, a northward boundary current is predicted to about 4°N. North of this latitude, potential vorticity conservation leads to a weak cyclonic interior flow that feeds a southward DWBC (Fig. 2).

In this model, a substantial eastward current along the equator is not reproduced. Johnson et al. (1991a) argued that elevated diapycnal eddy diffusivities at the equator could account for larger upwelling rates, which in turn justifies the eastward spreading of CDW. However, estimates of abyssal eddy diffusivities within 1° of the equator in the Indian Ocean have not revealed elevated levels (Dengler and Quadfasel, 2002). An average eddy diffusivity in the order of $K_\rho = 2 \times 10^{-5} \text{ m}^2 \text{ s}^{-1}$ was found in the depth range between 500 and 2000 m.

Recently, Beal et al. (2000) observed a temporal reversal of the bottom circulation in the northern Somali Basin based on two sets of lowered ADCP and hydrographic measurements along 8°N. In June 1995, a southward DWBC with a transport

of 5 Sv was observed, in September the flow was northward with a transport of 2.6 Sv. The deep zonal density gradient across the interior of the basin also changed between the two occupations, implying a cyclonic circulation in June and an anti-cyclonic circulation in September. Apart from considering elevated eddy activity the authors suggested a strong barotropic component to the Great Whirl in September to cause the flow reversal in the bottom waters.

As part of the German contribution to the World Ocean Circulation Experiment (WOCE), a measurement program was carried out in the Indian Ocean Special Survey Area 2 (ISS2), located in the western Arabian Sea. The program consisted of three cruises between March 1995 and August 1995 (Fig. 3a) and a mooring array ICM7 deployed in the Somali Basin from April 1995 to October 1996 (Fig. 3b). In this paper, the bottom and deep circulations and their variability are discussed on the basis of the above data sets.

2. Data

On cruise M32, R/V *Meteor* completed three surveys in the Somali and Arabian Basin, predominately on repeated cruise tracks. The first leg

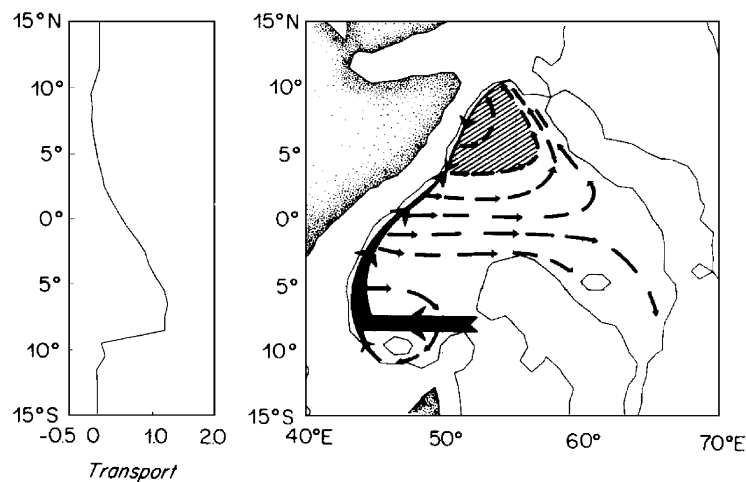


Fig. 2. Schematic illustration of the bottom circulation as predicted from the Stommel and Arons (1960) concept. The transport of the DWBC relative to a unit source is shown on the left. The schematic flow of the bottom water is shown on the right, with the basin outline being the 3800 m isobath used by Johnson et al. (1991a). The cyclonic recirculation of bottom water in the northern part is shaded (adapted from Johnson et al., 1991a).

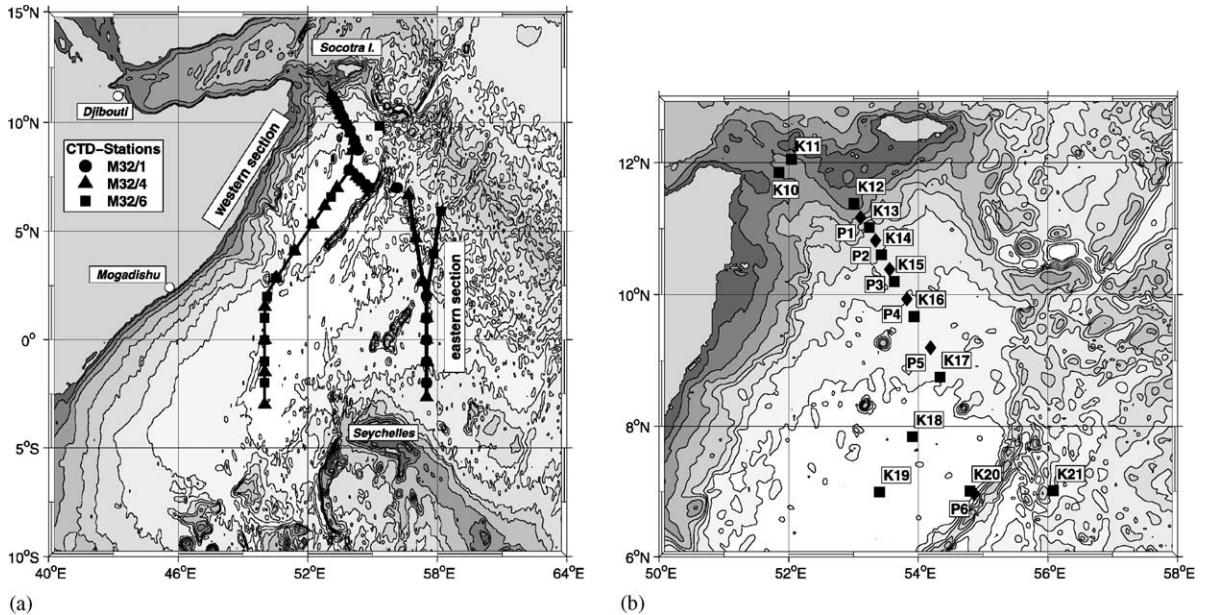


Fig. 3. (a) Locations of deep CTD casts collected in the Somali Basin during the three R/V *Meteor* cruises. Bottom bathymetry (Smith and Sandwell, 1997) shading increases from 5000 m (white) by 500 m to 3000 m then by 1000 m. (b) Position of moorings (K10–K21) and Pegasus transponder pairs (P1–P6) in the northern Somali Basin.

M32/1 was conducted during the transition from NE to SW-monsoon between March 26 and April 25, while two subsequent cruises, leg M32/4 and leg M32/6, were carried out in the early stage and fully developed SW-monsoon from June 8 to July 10 and from August 17 to September 19, respectively. In addition to the hydrographic surveys, an array consisting of 12 current meter moorings was deployed and nine Pegasus transponder pairs were installed during M32/1. Unfortunately, during all three cruises the vessel could not enter the Somali exclusive economic zone (EEZ) due to unresolved clearance situations. Hydrographic sections therefore were conducted outside the EEZ (Fig. 3a) and most of the moorings were set following the EEZ's boundary from 7°N to the continental shelf of Socotra Island (Fig. 3b).

Subsets of these observations were presented in several earlier publications. Quadfasel et al. (1997) determined the deep-water exchange through the Owens Fracture Zone on the basis of the deep hydrographic data. Schott et al. (1997) analyzed the summer monsoon response in the upper

1000 m using direct velocity measurements and hydrographic data. Apart from a monsoon response of the Great Whirl reaching to 1000 m depth, they found the Somali Current and the Great Whirl to be decoupled from the Arabian Sea. Instead, communication occurred predominantly through the Passage between Socotra Island and the African continent. Most recently Schott and Fischer (2000) discussed the winter monsoon circulation of the northern Arabian Sea and the Somali Current using the moored current observations.

The shipboard observations on all three cruises consisted of conductivity–temperature–depth dissolved oxygen (CTD- O_2) measurements and direct current measurements by a shipboard acoustic current Doppler profiler (ADCP), a lowered ADCP and a Pegasus profiler. CTD data were collected with a Neil Brown Mark III system, which was, along with the oxygen sensor, attached to a rosette with 21 Niskin bottles. Three bottles had to be left out to make room for the lowered ADCP (LADCP). The accuracy of the CTD- O_2 measurements meets the WOCE requirements set

in Joyce and Corry (1991). After calibration, the overall accuracy of salinity in deeper waters was better than 0.002 for all three cruises. Laboratory calibration of the temperature sensor prior to and after the cruises showed its accuracy to be within 0.002 K. Oxygen was measured with a Beckman sensor and calibrated using the O_2 values from the water samples determined by the Winkler method. Accuracy after calibration was better than $3.05 \mu\text{mol kg}^{-1}$. LADCP measurements were carried out using a RDI narrow-band 153 kHz ADCP (NBADCP), except in the first week of cruise M32/1, when a broad-band ADCP (BBADCP) was in use. The BBADCP failed to measure currents below 2000 m and was therefore replaced after station 28 (Schott et al., 1996). The data were processed using a method similar to that described in Fischer and Visbeck (1993). One modification included an interpolation of flagged bins when velocity data were available in preceding and subsequent bins, leading to a more accurate determination of the velocity integrated over time.

Shipboard ADCP data also were collected with a RDI narrow-band 153 kHz ADCP. R/V *Meteor* was equipped with an Ashtech 3D-GPS receiver, which substantially improved the data quality because a heading-dependent error of the Gyro compass could be corrected. For data processing, the CODAS3 software (Firing, 1991) was used. High-quality data were collected in the upper 350 m of the water column.

Two meridional repeat sections were occupied in the Somali Basin. The western section ran from 3°S , 50°E to Socotra Island, thereby sampling the center of the northern Somali Basin (Fig. 3a). The full section was completed during M32/4 and M32/6 only. The eastern meridional section along 57.5°E between 3°S and the Carlsberg Ridge was completed on all three cruises. Although station spacing was 30 nm or less on both sections, deep profiles were only collected every second or third station in some parts.

The mooring array WOCE ICM7 was deployed in April 1995 (M32/1) and retrieved with a chartered vessel in October 1996. The 11 moorings had a total of 57 Aanderaa rotor current meters (RCMs) and 7 self-contained ADCPs. The array

was made up of three elements. Two moorings (K10 and K11) were set up to monitor currents in the about 1000 m deep Socotra Passage (Fig. 3b). The results are reported in Schott et al. (1997) and Schott and Fischer (2000). A boundary current array (K12–K16) was deployed perpendicular to the isobaths of the continental slope south of Socotra Island. All moorings in the deeper water were equipped with RCMs at 2000 m, but additionally six instruments were placed at deeper levels to observe a possible boundary current at the northern continental slope. Finally, a triangular setup was chosen (K17–K21) in the central Somali Basin to resolve planetary wave propagation. This included a mooring close to the Chain Ridge (K20) with an instrument at 4000 m depths. The upper layer velocity records have been described by Schott and Fischer (2000). Here, the discussion focuses on the records from deeper than 2000 m.

Altogether, nine sets of Pegasus profiles were obtained during the three cruises. Pegasus is a free falling profiler that measures horizontal velocity (Spain et al., 1981). Six transponder pairs were deployed in the northern part of the Somali Basin. Their positions were chosen to interleave with the mooring array line (Fig. 3b). The remaining three were positioned along 57°E at 1°N , the equator and 1°S . The survey technique described by Send et al. (1996) was used for determining the transponder locations. The dropsonde was adjusted to have downward velocities of about 0.85 m s^{-1} and upward velocities of 0.5 m s^{-1} . The recorded travel times were converted to distances using a sound speed profile from a simultaneously measured CTD profile at the same position. After de-spiking, horizontal velocities were calculated and low-pass filtered with a 50 m cut-off wavelength to remove small scale instrumental noise. Send (1994) found the absolute error of the Pegasus velocities after filtering to be less than 0.02 m s^{-1} .

The above described variety of different direct current observations at similar positions made it possible to quantify uncertainties inherent in the different instruments by an inter-comparison study. It is presented in detail in Appendix A. In summary, the RCM and Pegasus velocities agreed

to within 1.5 cm s^{-1} , but the LADCP data showed larger uncertainties with the 95% confidence being 9 cm s^{-1} and a bias of 0.4 cm s^{-1} in both velocity components. We will refrain from a description of the abyssal circulation on their basis. However, depth-averaged Pegasus and LADCP velocities compared well having a standard deviation of only 0.81 cm s^{-1} . In Section 3.2, these measurements will be used to reference geostrophic currents.

3. Observations

3.1. Bottom and deep water masses

Circumpolar Deep Water enters the Somali Basin via the Amirante Passage, having potential temperatures between $0.8^\circ\text{C} \leq \theta \leq 1.1^\circ\text{C}$, salinities lower than 34.725 and dissolved oxygen values higher than $175 \mu\text{mol kg}^{-1}$ (Johnson et al., 1998). This water occupies the Somali Basin at depths greater than 4000 m (Figs. 4 and 5). However, for reasons mentioned below, we will distinguish between bottom and deep water, i.e. CDW and IDW, below and above the 3500 m isobath throughout this presentation.

The coldest, least saline and most oxygen rich bottom water is found below 4900 m depth south of the equator in the western section (Fig. 4) in agreement with a southern entry point of CDW. At our southern section end minimum potential temperatures were just below 0.9°C and salinities less than 34.716. Johnson et al. (1998) reported maximum northward transport in the Amirante Passage at temperatures between 0.8°C and 0.9°C . Pre-WOCE hydrographic measurements (Fieux et al., 1986; Barton and Hill, 1989) confirm the presence of water with temperatures of 0.8°C at about 4700 m and colder water in the Amirante Passage. The absence of the cold water in our measurements suggests significant warming of the inflow water through vertical mixing south of 3°S . This is consistent with temperature observations in the bottom water within the Amirante Passage, which increased by 0.04°C over a meridional distance of 100 km (Johnson et al., 1998).

Between the equator and about 5°N in the western section (Fig. 4), near-bottom temperatures

and salinities gradually increase. Meridional gradients of the bottom water mass properties are largest in the vicinity of topographic features between 2°N and 4°N . As indicated in Fig. 3a, the varying bathymetry is due to the wider continental slope off Somalia crossing the section. At this latitude, a northward spreading of CDW near the bottom is further constricted by the Chain Ridge to the east. However, TOPEX/POSEIDON and ship depth sounding derived bathymetry from Smith and Sandwell (1997) (Fig. 3a) indicate several gaps with maximum depths larger than 5000 m between the continental slope and the Chain Ridge through which the bottom water can spread northward.

North of 5°N , the western section runs central through the northern Somali Basin. Horizontal near bottom property distributions are roughly constant and minimum temperatures of 0.96°C and salinities of 34.718 are observed. A patch of colder, less saline and oxygen-rich water at the foot of the continental slope of Socotra is visible in the data from June 1995 (Fig. 4). However, this patch was not observed during the other two cruises and is thus not a persistent feature.

In the eastern part of the basin along 57.5°E minimum temperatures and salinities just below 1°C and 34.72 were measured close to the bottom (Fig. 5). Maximum depths in this part of the basin hardly exceed 4600 m, which appears to be too shallow to permit the spreading of dense CDW. Some deep gaps in the sea floor close to the Carlsberg ridge are seen in the Hydrosweep bathymetric data plotted in Fig. 5. No CTD measurements are available from inside these gaps.

There are two possible explanations for the observed property distributions in the CDW. The lack of cold CDW north of 5°N may be due to the longer route the water takes to reach the northern part of the basin. This is in agreement with the Stommel and Arons (1960) framework, which predicts a weak cyclonic bottom circulation in the northern Somali Basin (Fig. 2). Another possibility is that north of the equator enhanced vertical mixing in the abyss leads to a different vertical advection–vertical diffusion balance in the deep water, thereby altering the property

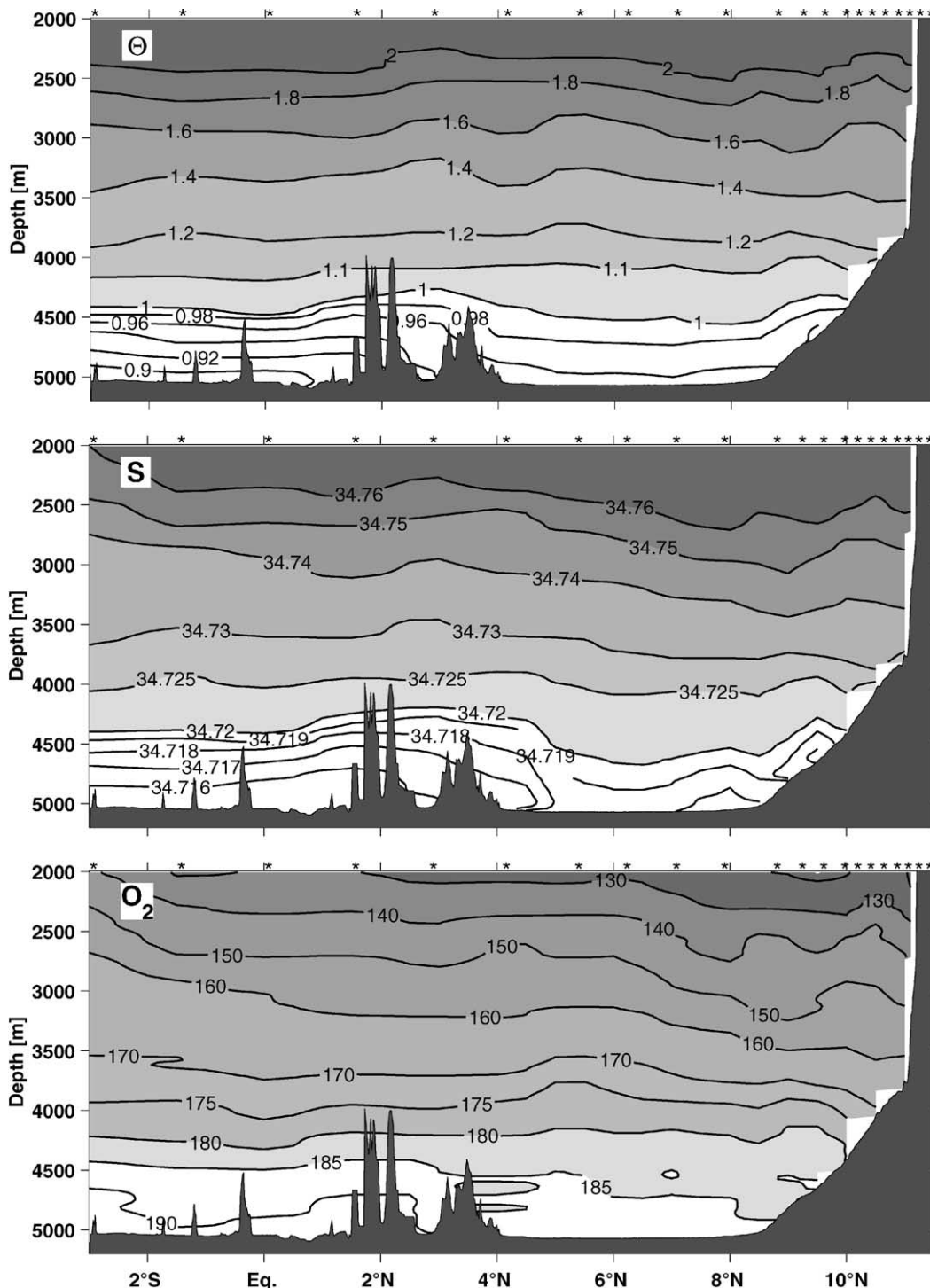


Fig. 4. Distribution of potential temperature (°C), salinity (PSS-78) and dissolved oxygen ($\mu\text{ mol kg}^{-1}$) along the western section (Fig. 3) during June 1995 (M32/4).

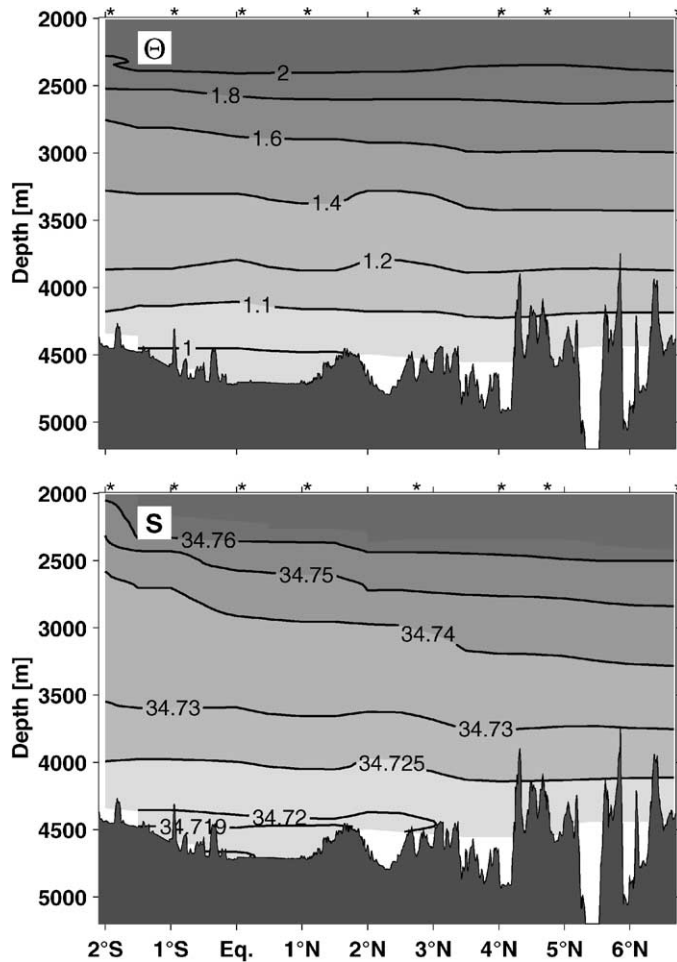


Fig. 5. Distribution of potential temperature and salinity along the eastern section during June 1995.

distribution. Some suggestions for the latter idea will be discussed in Section 4.

Above the CDW to 2000 m, the deep water is characterized by the higher salinities and lower oxygen values of the Indian Deep Water. The imbalance of volume transport in the Amirante Passage reported by Johnson et al. (1998) requires a westward advection of IDW north of the Amirante Passage, which has to pass through the western section. They determined a southward flow in the Amirante Passage between the isotherms $1.4^{\circ}\text{C} \leq \theta \leq 1.9^{\circ}\text{C}$, located at 3500 and 2400 m, respectively, having salinities between

34.73 and 34.745. Dissolved oxygen was between 150 and $170 \mu\text{mol kg}^{-1}$ (Fig. 6).

In the deep-water layer above about 3500 m, there is a pronounced meridional gradient in salinity and oxygen content (Fig. 4). At constant depths, salinity increases towards the north whereas oxygen decreases. In the northern part of the section, mesoscale displacements of the isotherms are seen. Here, the θ - S characteristics (Fig. 6) show a continuous linear relation in the bottom and deep water, whereas a change in slope at $\theta = 1.4^{\circ}\text{C}$ is visible in the profiles from south of the equator, becoming more distinct as the

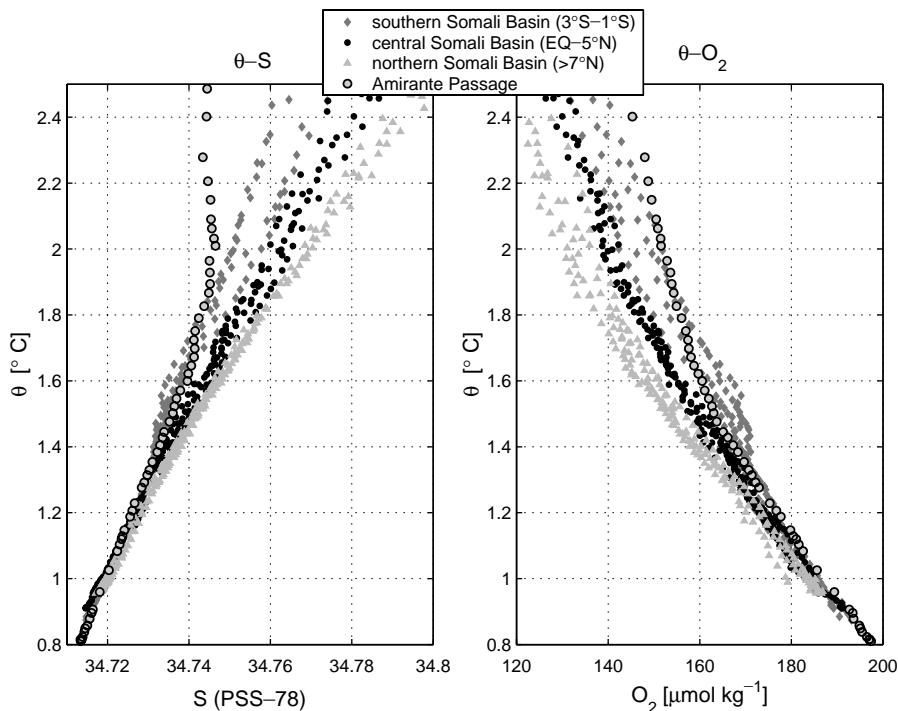


Fig. 6. Property curves of salinity (left panel) and oxygen (right panel) versus potential temperature from the western and eastern section.

southern most latitude is approached. Here, salinity is nearly constant between $1.4^{\circ}\text{C} \leq \theta \leq 1.6^{\circ}\text{C}$.

In contrast, the θ - O_2 characteristics of the western and eastern profiles north of about 1°S have a near linear relation to about $\theta = 1.8^{\circ}\text{C}$ (Fig. 6). In the northwest, there is a greater decrease in oxygen with increasing temperature than in the other parts of the basin. At $\theta = 1.6^{\circ}\text{C}$ a curvature of the θ - O_2 distribution is pronounced, leading to a decreased decline of oxygen with increasing temperature. South of about 1°S , the near constant salinity characteristic between $1.4^{\circ}\text{C} \leq \theta \leq 1.6^{\circ}\text{C}$ is accompanied by a near constant oxygen distribution. In a meridional CTD section on 57°E (WOCE I7N) occupied by R/V *Knorr* in July 1995, the anomalous water properties in this temperature range were most pronounced at the continental slope of the Mascarene Plateau (not shown). Near constant salinity and oxygen properties of the water south of the equator between $1.4^{\circ}\text{C} < \theta < 1.6^{\circ}\text{C}$ also have been

observed in data near 3°S off the coast of Africa (Johnson et al., 1991a). With present data, deep water having similar salinity and oxygen characteristics is also discernible on the eastern flank of the Southeast Indian Ridge, at 30°S , Central Indian Ridge at 20°S , 18°S , and 12°S and Mascarene Plateau at 8°S (B. Warren, pers. comm., 2001), indicating a southern origin of this water.

The possible westward flow of this deep water makes it a candidate for the southward outflow through the Amirante Passage. However, the θ - S and θ - O_2 characteristics from the Amirante Passage (WOCE-IO2W section, R/V *Knorr*, Voyage 145-14 conducted during December 95 to January 96, CTD-stations 1199 and 1200) in Fig. 6 do not exhibit similar characteristics. Instead, a linear θ - S relation is found for temperatures lower than $\theta = 1.6^{\circ}$. Unless a substantial modification of this water mass takes place, it is unlikely that the water found at the continental slope of the

Mascarene Plateau and near 3°S off the coast of Africa participates in the southward flow through the Amirante Passage.

3.2. Velocities and geostrophic transports

3.2.1. Direct velocity measurements

Deep profiles of horizontal velocity using a Pegasus drop sonde were collected in the northern Somali Basin and within 1° of the equator during all three R/V *Meteor* cruises. To describe the bottom circulation in the northern Somali Basin, vertical averages of horizontal velocity were calculated between 3500 m depth and the bottom.

Between April and August, the bottom circulation north of 9°N tends to become more easterly (Fig. 7). Velocities above 5 cm s⁻¹ are observed, but a clear and consistent circulation pattern does not really evolve. Beal et al. (2000) found a cyclonic bottom circulation in June 1995 and a reversed bottom circulation in September 1995 below 3800 m. Our observations contrast their results. The velocities from the June section, recorded within a week of the observations reported by Beal et al. (2000), rather suggest an anticyclonic circulation and there is no indication of a flow reversal between the surveys from June and August. Beal et al. (2000) suggest a strong barotropic component of the Great Whirl to cause the flow reversal in the bottom water. However, during the M32/4 section occupation from June 16 to June 20, the Great Whirl was not pronounced.

Bottom velocities within 1° of the equator show a strong eastward flow between 3500 m and the

bottom in April, in particular at and to the south of the equator (Fig. 8). In June, there was no clear circulation pattern while in August the flow had reversed relative to April and southeastward velocities of about 3 cm s⁻¹ were observed.

Although the horizontal and temporal resolution of the direct velocity measurements is limited at the equator, it is fair to say that they do not show a stationary eastward current as suggested by Johnson et al. (1991a). Instead, we find time-dependent currents at the equator with a reversal of flow direction between occupations. Luyten (1982) analyzed four deep current-meter time series (3600 m) moored at the equator and at 1.5°N between 51°E and 57°E from May to December in 1978. The velocity time series were dominated by fluctuations having periods longer than 50 days. On average, Luyten (1982) found northeastward flow of about 1 cm s⁻¹ over the deployment time span of nearly 8 months.

3.2.2. Geostrophic velocities

To investigate the abyssal flow in the northern Somali Basin, the geostrophic velocity fields and transports between 7°N and the continental shelf of Socotra was determined. In the south the section was terminated at the Chain Ridge (Fig. 3a) and is therefore closed to the east below the sill depths of the Owen Fracture zone. Past investigators have had difficulties when referencing geostrophy in the northern Somali Basin. Fieux and Swallow (1988) found extremely large abyssal geostrophic velocities of 23 cm s⁻¹ using a zero velocity surface at 2000 m depth. Due to eddy

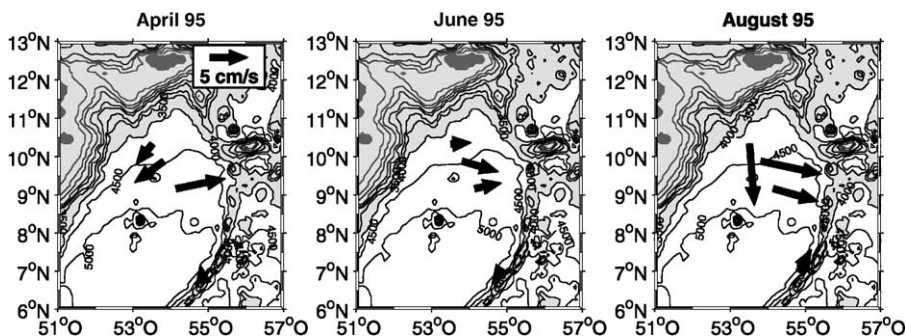


Fig. 7. Bottom velocity vectors, averaged from 3500 m depth to bottom, from Pegasus profiles in the northern Somali Basin.

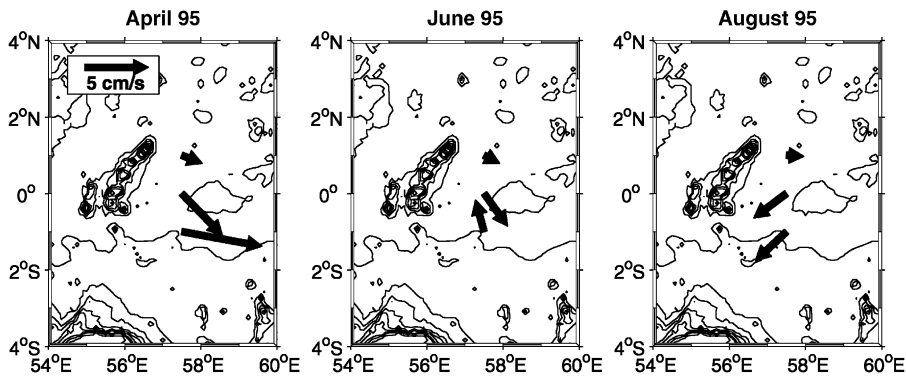


Fig. 8. Bottom velocity vectors from Pegasus profiles from the eastern section averaged between 3500 m and the bottom.

noise, Johnson et al. (1991a) refrained from estimating geostrophic transport in the northern part of the basin.

On two of the three R/V *Meteor* cruises LADCP current profiles were measured at each station using a NBADCP. The good agreement between the barotropic, i.e. depth-averaged velocities measured by the Pegasus drop sonde, and the barotropic velocities of the NBADCP described in Appendix A encouraged us to use the latter for referencing the geostrophic velocities. However, the depth averaged LADCP velocities contain current components that are not accounted for in the geostrophic approximation, especially tidal currents, Ekman and cyclostrophic components as well as a possible velocity bias. These have to be removed prior to referencing. The procedure to this and an error estimate is briefly described in Appendix B.

The results are shown in Fig. 9. In general, the deep geostrophic velocity field is dominated by baroclinic motion of decreasing horizontal scale toward the continental shelf. Going northward from 10°N, there are several reversals in flow direction below 1500 m depths. These features were also seen in the LADCP profiles and are therefore not artificially arising from dense CTD station spacing. Furthermore, they are consistent with the Pegasus measurements presented in Fig. 7.

Overall, the flow field south of 10°N in August appears to be less structured compared to June. Below 1000 m to the bottom, eastward flow was

found between 8°N and 10°N and westward flow further to the south. However, this picture may only result from the large gap in station spacing between 7.5°N and 9°N. The upper water column in August is dominated by the presence of the Great Whirl. Its vertical rotation axis was located at 10°N and a substantial part of the eastward recirculation took place on the shelf of Socotra, not included in these sections. One peculiar feature is the lack of vertical shear of geostrophic velocities between station 88 and 89 at the eastward flowing flank of the Great Whirl. In the June section, strong eastward flow with velocities exceeding 30 cm s^{-1} was present between 1000 and 1500 m near 10°N. Velocity time series from 1000 m at K15 indicate that these large eastward velocities persisted between mid-June to mid-August, while westward velocities of the same magnitude were observed throughout October.

3.2.3. Geostrophic transport estimates

Cumulative geostrophic transports were calculated by averaging the geostrophic transport sections on neutral density surfaces and integrating them vertically upward (Fig. 10). In the deep part of the water column, bottom wedges were treated by least-square-fitting temperature and salinity to the bottom triangle (Wunsch, 1996, p. 220). No adequate procedure was found to treat the deep reaching wedges at the continental shelf of Socotra above 2000 m, which were thus neglected. Furthermore the southernmost station

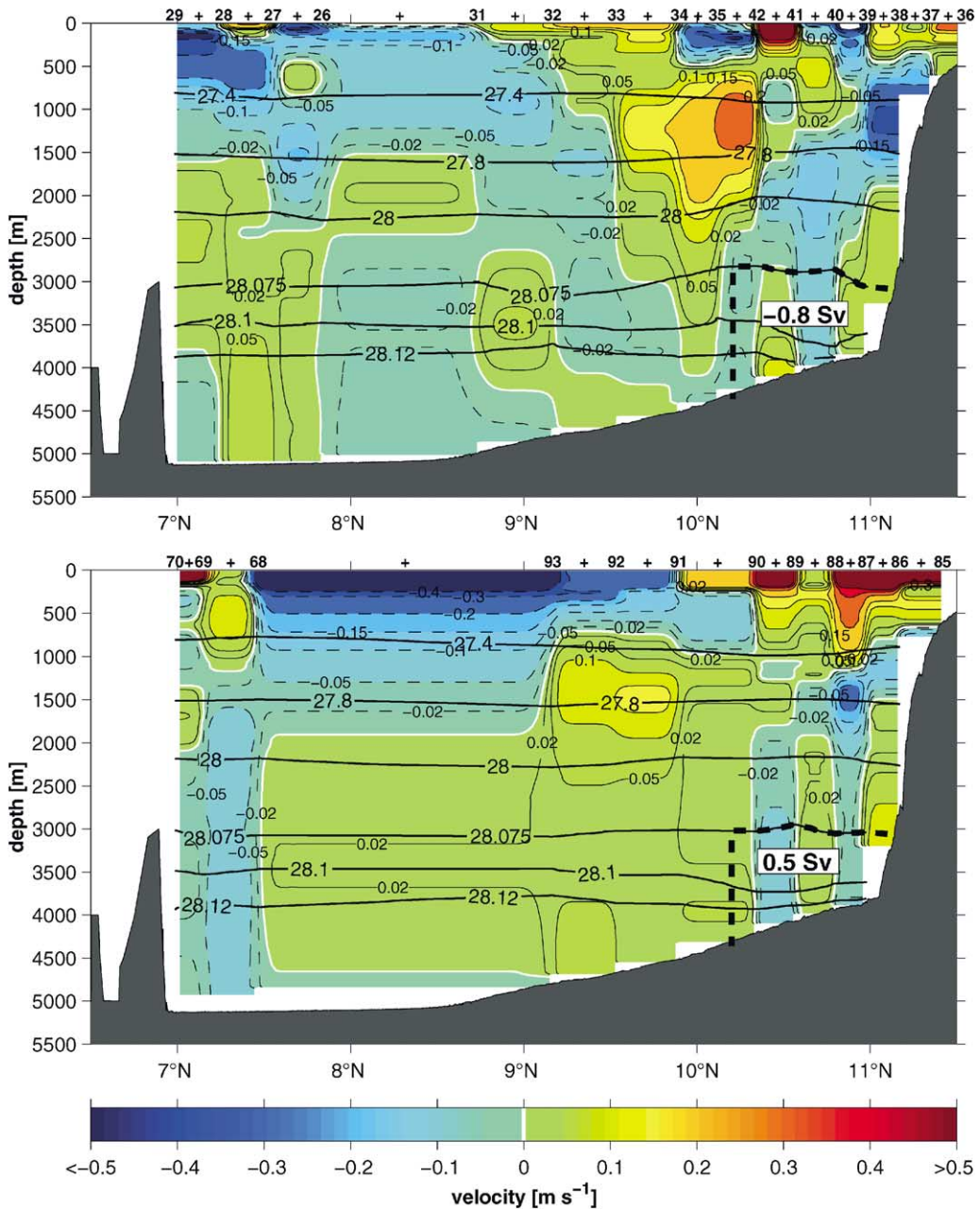


Fig. 9. Geostrophic velocities in the northern Somali Basin from ship sections (Fig. 3a) during June (upper panel), and August (lower panel). Positive velocities are eastward. Thick contours represent neutral density surfaces in kg m^{-3} . Filled bathymetry is taken from a Hydrosweep echo sounder data recorded during the cruises. Velocities are referenced by vertically averaged ADCP currents (see text for details). Dashed lines indicate area used for DWBC transport estimates. The numbers along the tops mark the positions of CTD stations, while pluses mark mid-points between stations.

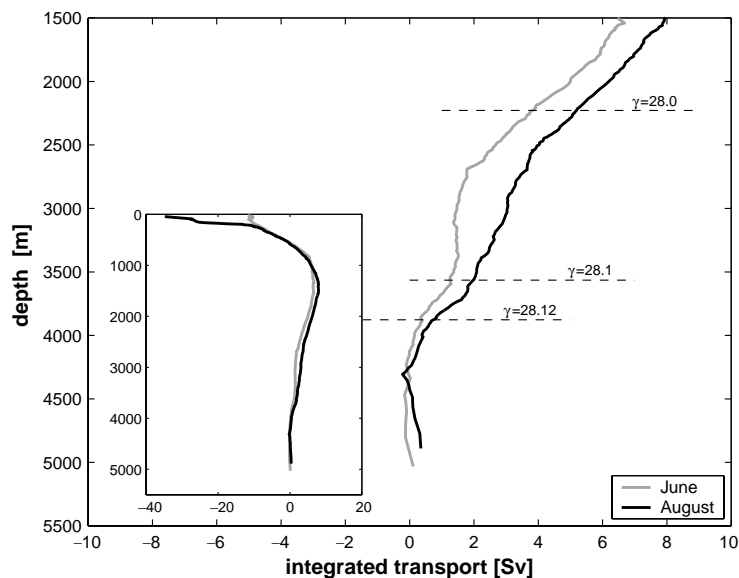


Fig. 10. Cumulative transports between 7°N and the Socotra Island from ship sections averaged on neutral density surfaces against their section average depth. Selected neutral density surfaces are indicated by the dashed line.

was extended by 8 km to the east. The sections are therefore closed below 3800 m by topography.

Despite the strong changes between the individual velocities on both sections, the integrated transport profiles from June and August are remarkably similar below about 300 m depth (Fig. 10). In both realizations a net eastward transport through the section is found from the bottom to about 1500 m depth and westward transport at shallower levels. In the upper 400 m, a large westward transport of -10 Sv and -35 Sv over the section is obtained for the June and August sections, respectively. Parts of this westward flow may balance the outflow through the Socotra Passage, which was between 4 and 6 Sv between the surface and 1000 m depth (Schott et al., 1997). However, especially during August 1995, large parts of the eastward flowing Great Whirl transport took place over the Socotra shelf (see Fig. 9 or Schott et al., 1997), which is not included in our estimate.

The skill of the applied referencing method is demonstrated by the small imbalance found below the neutral density surface $\gamma = 28.12$ kg m $^{-3}$, located below 3800 m in both realizations. Here, no net transport is expected. The imbalances

found in the June and August sections were just 0.3 and 0.8 Sv, respectively (Fig. 10). However, it cannot be ruled out that parts of the imbalance found for August also might originate from the fact that the section was not collected synoptically. A temporal gap of 7 days existed between the occupation of stations 68 and 93. From a statistical viewpoint, the expected imbalance adds to 1.3 Sv using an error in velocity of 1.2 cm s $^{-1}$ as derived in Appendix B. Referencing the geostrophic velocities at $\theta = 1.6^\circ\text{C}$, which corresponds to an average depth of 3000 m used by other investigators (e.g. Johnson et al., 1991b; Quadfasel et al., 1997), leads to an imbalance of -2.5 Sv for June and 1.6 Sv for August for the same depth range.

In the bottom water layer below the neutral density surfaces $\gamma = 28.1$ kg m $^{-3}$, i.e. below 3500 m depths, net eastward transports were 1.4 ± 0.5 Sv in June and 2.1 ± 0.6 Sv in August. Transport error estimates are based on the uncertainty of reference velocity (Appendix B). These results are in good agreement with the exchange of bottom water between the Arabian Basin and the Somali Basin determined by Quadfasel et al. (1997) using data collected on

the same cruises east of the Owens Fracture zone. Both integrated transport profiles in Fig. 10 show the largest transport gradients in the column from 3500 to about 3800 m, just above the sill depth of the Owen Fracture zone.

The deep water column between 2000 and 3500 m is represented between the neutral density surfaces $\gamma = 28.00 \text{ kg m}^{-3}$ and 28.1 kg m^{-3} . Here, an eastward transport of $3.6 \pm 2.3 \text{ Sv}$ in June and of $4.0 \pm 2.4 \text{ Sv}$ in August is obtained. The results of these two realizations therefore disagree with the hypothesis of westward flow of IDW in the northern Somali Basin, which may eventually participate in the outflow of deep water through the Amirante Passage found by Johnson et al. (1998).

3.3. Moored array current observations

The WOCE ICM7 array contained seven rotor current meters moored at depths larger than 2000 m. The time series of six of these observations are shown as current vectors in Fig. 11. The

seventh RCM moored at K15 in 4200 m lost its rotor 7 months after deployment and will not be considered.

The most prominent feature common to all time series is the energetic intra-seasonal variability. The amplitudes of the fluctuations can exceed 10 cm s^{-1} , but are usually about 5 cm s^{-1} . The variance-preserving frequency spectrum calculated from the deep velocity records shows a pronounced maximum at the 30- to 50-day period band (Fig. 12), representing the dominant time scale of the fluctuations. They are present also in the shallower records (not shown) and their baroclinic character is indicated by reversals of phase between the shallow and deep records. Meridional variance of the fluctuations exceeds zonal variance.

These intra-seasonal fluctuations are also reported from TOPEX/POSEIDON altimetry data from the northwest Indian Ocean, in the region from 5°N and 11°N and from off the coast of Somalia to about 60°E (Eigenheer, 1997; Brandt et al., 2002). They have maximum amplitudes

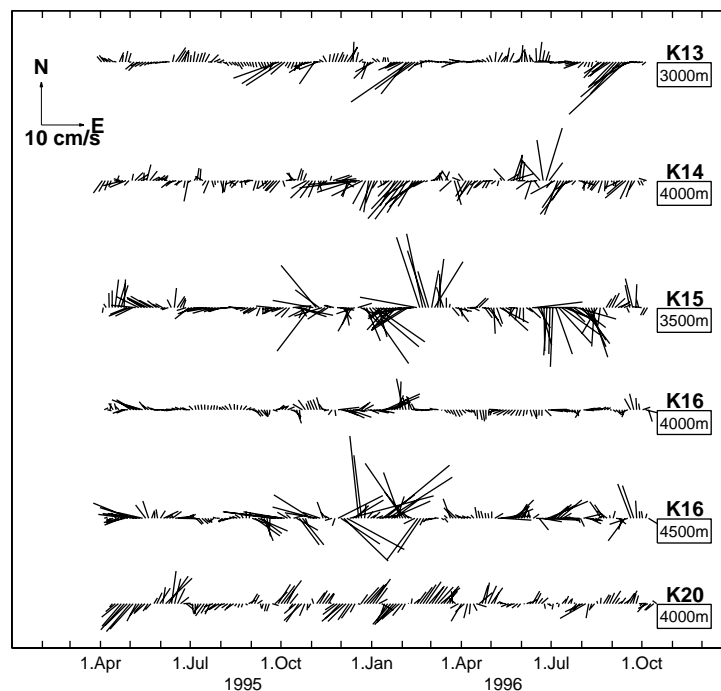


Fig. 11. Vector time series of 40-h averaged deep velocity measurements in the northern Somali Basin. Barotropic tidal currents were subtracted prior to averaging.

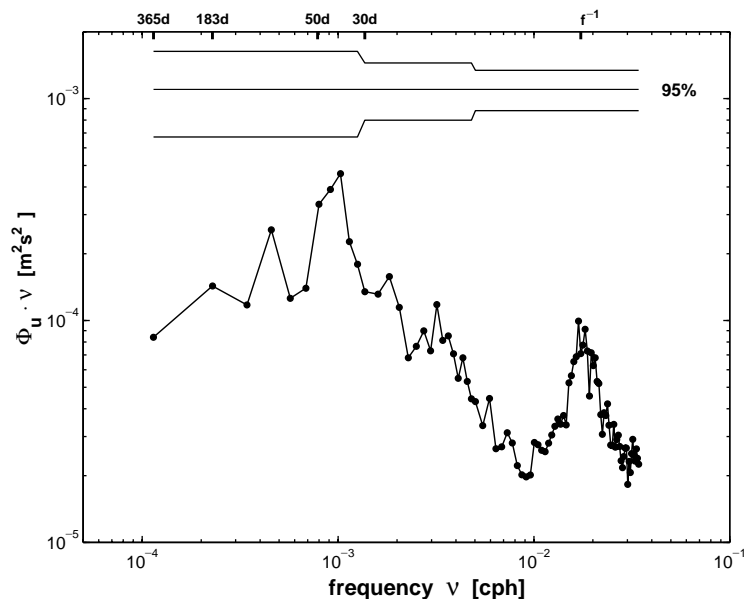


Fig. 12. Variance-preserving frequency spectra of horizontal velocity calculated from the six deep records from below 3000 m depth from the northern Somali Basin.

during the southwest monsoon period and show westward phase propagation. Strong intra-seasonal current variability dominated by meridional fluctuations with periods between 30 and 50 days in the same area was found by Sengupta et al. (2001) in the data from a modular ocean model setup for the Indian Ocean north of 30°S. An interesting result here is that the current fluctuations were also present in a model run forced with seasonal wind (periods 90 days or greater) only. This indicates that the fluctuations are generated by the instability of the large-scale circulation rather than forced directly by the wind. A detailed description of the observed 30- to 50-day fluctuations will be presented in a separate paper.

The large amplitude 30- to 50-day fluctuations in the velocity field of the abyssal Somali Basin may account for the drastic changes found in the Pegasus and geostrophic velocities as well as explain the variability found in previous investigations (Johnson et al., 1991a; Beal et al., 2000). However, especially the deep time series at K14 and to a lesser extent K13 indicate a predominant current direction, which will be discussed below.

Furthermore, the velocity time series provide means to investigate the seasonal cycle.

3.3.1. Average velocities and transports

Significant average southwestward velocities were found at K13 and K14, amounting to 1.3 and 2.1 cm s^{-1} , respectively (Table 1). Progressive vector diagrams of the velocity records in Fig. 13 show a drift past the RCMs of 1100 km at K14 in 4000 m depth and 850 km at K13 in 3000 m depth during the deployment time span. At K15 and K16 only marginally significant mean flows were observed. However, the drift past these locations exhibits circular movement that is less pronounced in the drift of the northern records. No significant average velocity was found at K20. Velocity variance is oriented along topography at K13 and K14. At K15 and K16, velocity variance ellipses are zonally oriented and the variance generally increases. An exception is the record in 4000 m depth at K16, where velocities are generally lower than those of surrounding records.

The average bottom circulation in the northern Somali Basin is thus cyclonic, with a boundary

Table 1

Running annual averages of the mean flow in maximum flow direction (\bar{u}), their standard deviation $\sigma(\bar{u})$ estimated by dividing the standard deviation of the velocity records by the square root of the degrees of freedom and average flow directions of the deep velocities times series

| Mooring no. | Depth (m) | $\bar{u} \pm \sigma(\bar{u})$ (cm s ⁻¹) | Direction of mean flow (°) | Degrees of freedom | $\sigma(u)$ (cm s ⁻¹) |
|-------------|-----------|--|-------------------------------|--------------------|-----------------------------------|
| K13 | 3000 | 1.31 ± 0.90 | 265 | 15 | 3.47 ^a |
| K14 | 4000 | 2.05 ± 1.11 | 225 | 15 | 4.32 |
| K15 | 3500 | 1.20 ± 1.12 | 201 | 19 | 4.91 |
| K16 | 4000 | 0.57 ± 0.53 | 78 | 16 | 2.11 |
| K16 | 4500 | 1.31 ± 1.08 | 38 | 17 | 4.43 |
| K20 | 4000 | 0.38 ± 1.14 | 30 | 14 | 4.27 |

^aThe standard deviations in the direction of the average flow is indicated by $\sigma(u)$. Tidal currents were removed prior to averaging.

current in the northwest corner Fig. 14. Here, on the continental slope of Socotra, the flow is southwestward and follows the topography. Highest speeds are seen at the foot of the continental slope, but about 1100 m above the bottom at K13 the mean flow is not significantly different from zero. These characteristics are typical for a deep western boundary current (e.g., Warren, 1981a).

Even though there is only a limited number of deep time series covering the average southwestward flow close to the continental slope of Socotra, an estimate of the DWBC transport is attempted. The boundary current is assumed to encompass the area north of the position of K15 and below 3000 m depth (see Fig. 14). Any use of interpolation schemes is unwarranted due to the limited data resolution. Instead, the area is simply linear distributed, assigning 40% of the total to each of the records at K13 and K14 and 20% to the record at K15.

As expected, the resulting time series of DWBC transport shown in Fig. 15 is dominated by 30- to 50-day fluctuations. For short periods of a few days, maximum southwestward transports of 14 Sv and northeastward transports of 10 Sv are obtained, showing the influence of the Rossby waves. On the basis of the crude assumptions above, an annual average transport and a standard deviation of the average of 2.0 ± 1.3 Sv in southwestward direction is obtained. The standard deviation of the transport is 3.7 Sv.

To partially verify the assumptions for the moored transport calculations, the geostrophic

transports were calculated from the June and August sections over the same horizontal distance below the neutral density surface $\gamma = 28.075 \text{ kg m}^{-3}$, enveloping the same area as used for the transport time series (see Fig. 9). In June and August, a southwestward transport of -0.78 ± 0.53 Sv and of 0.52 ± 0.67 Sv were obtained, respectively (Fig. 15). The average mooring transport estimates during the time of the section occupations were 0.17 Sv in June and 0.40 Sv in August, both in southwestward direction. The mooring estimate in June is slightly above the geostrophic estimate, but within the uncertainties discussed. In summary, the results of both methods are in general agreement, giving some confidence in the mooring transport estimates.

3.3.2. Seasonal cycle

Previous investigators have suggested a monsoon response in the abyss of the northern Somali Basin. The velocity time series from the ICM7 array provide means to investigate the depth penetration of the response to the seasonal forcing of the monsoon winds in the northern Somali Basin. Amplitude and phase of the seasonal signal were determined by fitting an annual harmonic along-shore current component of the time series using minimum variance criteria. Although a single amplitude and phase of an annual harmonic determined from a 18-month record is not statistically significant when the described variance of the signal is low, the results presented in Fig. 16

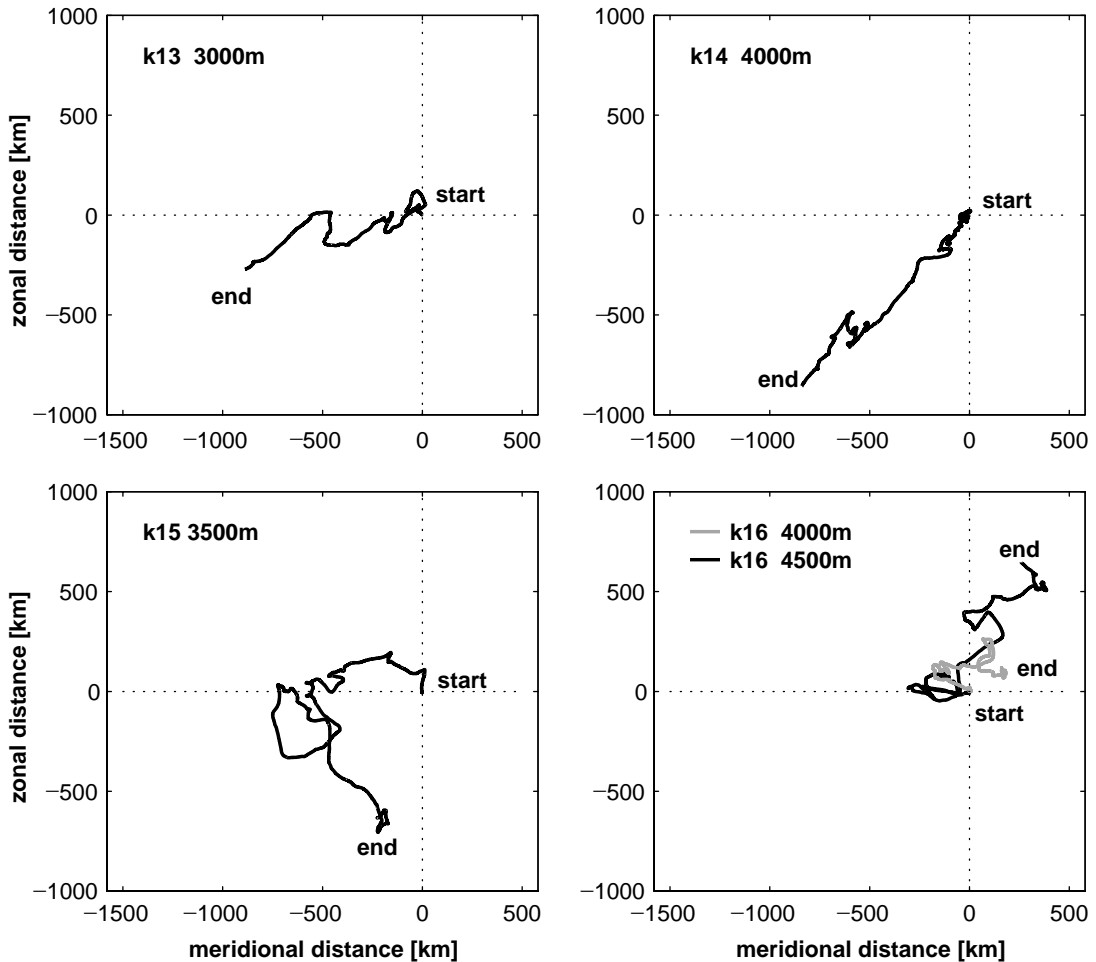


Fig. 13. Progressive vectors diagrams of the deep velocity records in the northern Somali Basin.

show consistent horizontal and vertical patterns along the section.

The seasonal cycle is most pronounced in the upper 200 m of the water column, where amplitudes exceed 40 cm s^{-1} . Two maxima with a 180° phase relationship occur between 7°N – 9°N and 10°N – 11°N , representing the contribution of the Great Whirl. Here, the annual signal contributes to more than 30% to the total variance of the time series. However, the northward propagation of the Great Whirl in 1995 and its early instability in September 1996 (Wirth et al., 2002) will reduce the amplitude and described variance of the seasonal signal locally.

There is a strong decrease of amplitude and contained variance of the annual signal with depth. At about 400 m, the amplitude drops off to below 5 cm s^{-1} . In the interior northern Somali Basin between 7°N and 10°N , amplitudes of less than 1 cm s^{-1} are found below about 1500 m. Described variance is below 5% for this part of the water column, indicating that the abyssal circulation in the interior Somali Basin is only marginally affected by the seasonal wind forcing. Instead, variance is dominated by the 30–50 day Rossby waves. These results do not confirm the hypothesis of Beal et al. (2000) who suggested a strong barotropic component of the

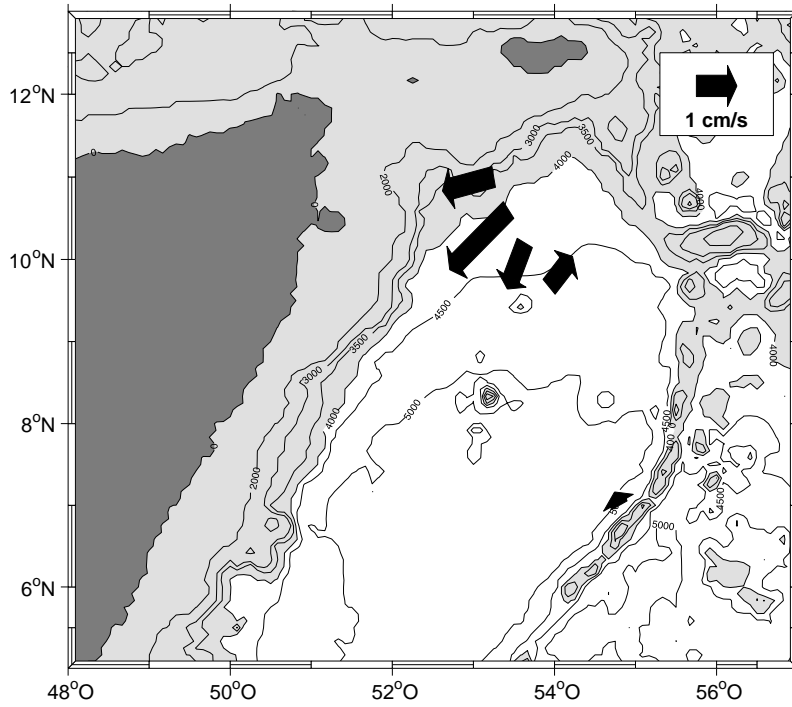


Fig. 14. Vectors of the average velocities calculated from the time series below 3000 m from the northern Somali Basin.

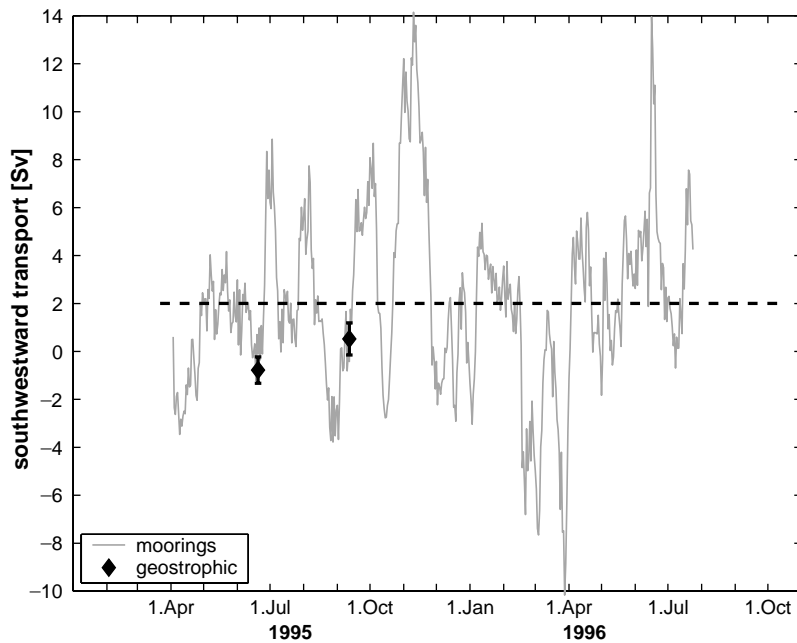


Fig. 15. Transport calculated from the moored time series (solid line) and geostrophic transports from the June and August cruise. Dashed line indicates annual average transport.

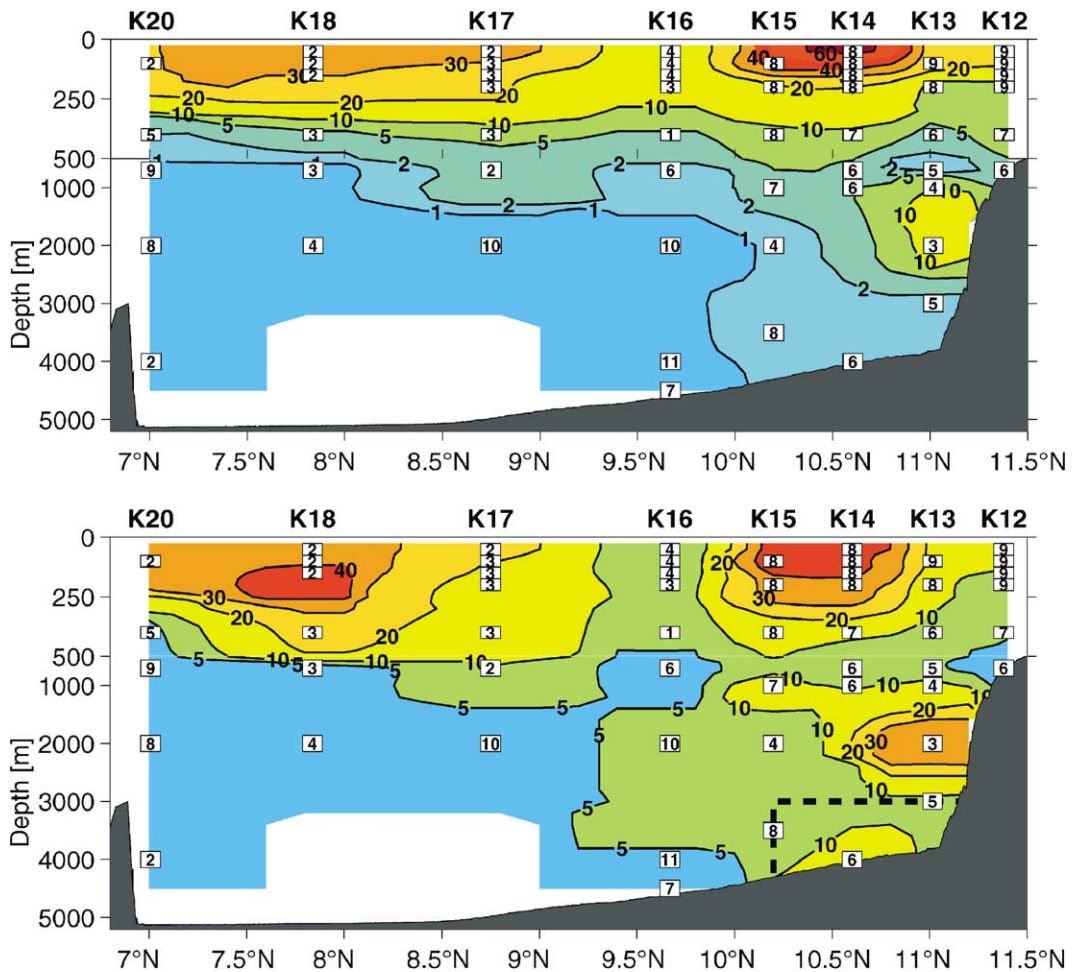


Fig. 16. Results from annual harmonic analysis. Upper panel displays amplitude of annual harmonic in cm s^{-1} . The lower panel shows described variance in % (contoured). Phase in months of the year are indicated by small numbers. Dashed lines indicate area used for DWBC transport estimates.

Great Whirl to cause a reversal in the bottom circulation.

However, amplitudes and contained variances increase towards the continental shelf. The amplitude of the annual signal at K13 increases from 1.6 cm s^{-1} at 700 m depths to 9.4 cm s^{-1} at 1000 m depths. At 2000 m, an amplitude of 10.5 cm s^{-1} was determined. Described variance at 1000 and 2000 m is 16% and 38%, respectively. Furthermore, the phase relationship of the deep amplitude maximum is reversed to the annual signal found in the upper water column. Whereas maximum northeastward velocities in the upper

ocean are observed in September, maximum southwestward velocities are found at 1000 and 2000 m. At 3000 m, amplitude is again strongly reduced and amounts to less than 2 cm s^{-1} .

The strong baroclinic response of the seasonal cycle close to the northwest boundary may be explained by the reflection of long Rossby waves of annual period. Brandt et al. (2002) showed that first and second vertical mode long annual Rossby waves propagate westward across the southern Arabian Sea. They are radiated from the western side of the Indian subcontinent and are continuously forced by the action of the wind curl field

over the central Arabian Sea. In TOPEX/POSEIDON altimetry data, these waves are most pronounced between 6° and 10°N and can be traced all the way to the coast of Somalia. At the northwest boundary, they will reflect into short Rossby waves and off equatorial coastal Kelvin waves, retaining the vertical mode of the incident wave. The short Rossby waves are generated to balance the cross-shore mass flux (e.g., Liu et al., 1999). Due to frictional effects, they will decay quickly away from the shelf and will not affect the interior of the Somali Basin as suggested in Fig. 16. Thus, they act only to redistribute mass along the boundary.

4. Summary and concluding remarks

The structure and dynamics of the abyssal circulation in the Somali Basin is explored on the basis of CTD and direct velocity measurements from shipboard surveys carried out during three stages of the SW monsoon in 1995 and deep velocity records from the WOCE mooring array ICM7 deployed in the northern Somali Basin between April 1995 and October 1996. To account for the Circumpolar Deep Water and the Indian Deep Water as two different abyssal water masses in the Somali Basin and their linked circulation, we discriminate between the bottom water below 3500 m depths and the deep water in the layer between 2000 and 3500 m depths.

Bottom water having a transport of 1.0–1.7 Sv enters the Somalia Basin via the Amirante Passage (Johnson et al., 1998). Property distribution along a meridional section in the western Somali Basin show the lack of dense CDW in the northern Somali Basin north of 5°N . Largest meridional gradients in the property distributions are found between 2°N and 4°N . However, a stationary eastward bottom current along the equator was not confirmed by direct velocity observations. Instead, time dependent currents with flow reversals between April and August are observed.

The most pronounced signals in the deep velocity records from the northern Somali Basin were baroclinic intra-seasonal fluctuations with periods of 30–50 days. Amplitudes associated with

the fluctuations were above 5 cm s^{-1} . Despite the large variability, statistically significant average southwestward velocities following the orientation of topography of 1.3 cm s^{-1} at 11°N and 2.0 cm s^{-1} at 10.6°N were determined from the deep records close to the continental shelf of Socotra, suggesting the presence of a weak DWBC. At a distance of 100 km away from the continental slope, a cyclonic recirculation was indicated. The annual average DWBC transport, calculated from the velocity time series below 3000 m north of 10.2°N was estimated to be $2 \pm 1.3\text{ Sv}$ in southwestward direction. Temporal variability in the DWBC transport is large, predominately due to the 30- to 50-day fluctuations. The average southwestward DWBC transport must be balanced by northeastward flow in the interior of the northern Somali Basin.

This circulation is in general agreement with the circulation of the Stommel–Arons model for the northern Somali Basin derived by Johnson et al. (1991a) (Fig. 2), which predicts a cyclonic deep western boundary circulation for the northern Somali Basin. The model assumptions of a uniform upwelling in the Somali Basin leads to a weak southwest boundary-current transport south of Socotra Island. In contrast to this hypothesis, the average transport estimated from the observations exceeds the inflow into the Somali Basin.

The cross-basin exchange of bottom and deep water between the Somali and the Arabian Basin north of 7°N was determined from geostrophic calculations referenced by vertically averaged LADCP currents. In the bottom water layer, eastward transports into the Arabian Basin of $1.4 \pm 0.5\text{ Sv}$ in June and $2.1 \pm 0.6\text{ Sv}$ in August were obtained. A large fraction of these transports were determined in depths just above the sill depths of the Owen fracture zone. Despite the strong variability, horizontally integrated transport profiles were remarkably similar, indicating that the eastward transport of bottom water into the Arabian Basin may only be marginally affected by the 30- to 50-day fluctuations. The transport estimates basically agree with the exchange of bottom water through the Owen fracture zone determined by Quadfasel et al. (1997) who found an eastward transport of 2.3 Sv in June and 1.2 Sv

in August from data collected in the Arabian Basin on the same two cruises.

The bottom water circulation in the Somali Basin on the basis of the above results is summarized as follows. In order to sustain the cyclonic DWBC circulation cell in the northern Somali Basin, a large fraction of the bottom water inflow into the Somali Basin spreads northward across the equator. North of 7°N it leaves the Somali Basin at a depths above 3800 m and ventilates the abyss of the Arabian Basin. This circulation scheme contrasts the inferred bottom water circulation by Johnson et al. (1991a). However, elevated levels of diapycnal mixing in the abyssal northern Somali Basin can account for the observed meridional gradients in the property distribution and justify an increased northward transport of bottom water into the northern Somali Basin. In a separate paper we will show that elevated eddy diffusivities are indeed found in the abyss of the northern Somali Basin.

In the deep-water layer, eastward transports of 3.6 ± 2.3 Sv in June and 4.0 ± 2.4 Sv in August 1995 were determined from the cross-basin sections north of 7°N. South of this latitude, transports could not be determined due to the lack of referencing. However, the southward export of IDW through the Amirante Passage between 4 and 8 Sv determined by Johnson et al. (1998) implies a westward transport of deep water between the Mascarene Plateau and 7°N of about 8–10 Sv.

Between the continental slope of the Mascarene Plateau and about 1°N, a distinct deep water mass was found in the potential temperature range between $1.4^\circ\text{C} \leq \theta \leq 1.6^\circ\text{C}$ having a near-constant distribution of salinity and O_2 . A possibility for part of its origin is a mid-depths western boundary current flowing northward along the eastern side of the Central Indian Ridge and the Mascarene Plateau (B. Warren, pers. comm., 2001). Similar water properties in the same temperature range also have been observed by Johnson et al. (1991a) near 3°S off the coast of Africa, suggesting a possible westward advection of this water, perhaps as a westward jet south of the equator. How this anomalous deep water leaves the Somali Basin remains unclear. However, it would need to be

substantially modified to participate in the southward flow through the Amirante Passage, since water with similar θ -S and θ - O_2 characteristics is absent in the Passage. Additional evidence of westward flow of deep water south of the equator is reported by Warren and Johnson (2002) from farther to the east. They determined westward transports of 2.2 and 6.7 Sv through passages in the Ninetyeast Ridge at 5°S and 10°S, respectively.

Finally, an analysis of a seasonal cycle in the moored time series indicates that the abyssal circulation in the interior northern Somali Basin is only marginally affected by the seasonal wind forcing. Amplitudes and explained variances in the current records of less than 1 cm s^{-1} , and less than 5% respectively were found for the seasonal cycle below 1500 m. This suggests that the reversing interior bottom circulation in the northern Somali Basin reported by Beal et al. (2000) was probably due to higher frequency variability. However, amplitudes of the seasonal cycle of 10 cm s^{-1} were found between 1000 and 2000 m depths at the northern continental slope south of Socotra Island. It is possible, that this increase was associated with the arrival of the annual Rossby waves described by Brandt et al. (2002).

Acknowledgements

We thank the captains and crews of the R/V *Meteor* and GMMOS *Discovery* for their help during deployment and retrieval of the moored array and the shipboard measurements, as well as C. Meinke, U. Papenburg, H. Wüllner, U. Drübisch and A. Welsch for technical assistance during the field work. The routines for the harmonic tidal analysis were kindly made available by H. Mofjeld, PMEL and the CTD data from the Amirante Passage by G. Johnson, PMEL. We thank Bruce Warren for constructive criticisms that significantly helped to improve the manuscript. This study was supported by the Deutschen Forschungsgemeinschaft (R/V *Meteor*) and the Bundesminister für Bildung und Forschung (WOCE).

Appendix A

Due to the diversity of direct current observations at similar positions, an inter-comparison was performed to quantify uncertainties inherent in the different instruments. Velocity data from the moored RCMs, the Pegasus drop sonde and the NBADCP are compared.

Comparisons were performed from velocity measurements within a 25 m depth interval and a sampling time that did not differ by more than 2 h. Sanford (1991) showed the horizontal coherence wavelength of the abyssal internal wavefield to be in the order of 15–20 km for mid-latitude internal waves. To avoid the influence of negatively correlated internal waves, horizontal velocity comparisons were further restricted to instrument positions less than 10 km apart. Also, RCM velocities smaller than the rotor threshold of 2 cm s^{-1} were excluded in the comparisons.

The velocity differences between RCM measurements from moorings and Pegasus measurements showed a standard deviation of 1.5 cm s^{-1} (Table 2). Considering the 2-h averaging interval of the RCM's, this difference cannot be distinguished from variability of the internal wavefield. No bias was found between the Pegasus and RCM velocities. The standard deviation of the velocity differences determined between RCM and NBADCP measurements was 4.8 cm s^{-1} . A linear fit to the velocity differences of both components showed the absolute RCM velocities to be larger by 14% and an offset of 0.4 cm s^{-1} . At each transponder location, a LADCP profile was collected after the Pegasus dropsonde was launched. The dropsonde was deployed about 15 min prior to the rosette and surfaced not later

than 30 min after the end of the CTD cast. Velocity differences between the near simultaneously collected profiles of the two platforms had a standard deviation of 4.6 cm s^{-1} , similar to the RCM–LADCP comparison. A linear regression showed the Pegasus velocities to be larger by 11% and again an offset of 0.4 cm s^{-1} . These results did not change, when linear regressions were calculated for zonal and meridional velocity only.

The large standard deviation found in the LADCP comparisons implies that the NBADCP velocities have a 95% confidence level of about 9 cm s^{-1} . In both comparisons, the absolute velocities of RCMs and the Pegasus were more than 10% larger than velocities measured by the LADCP, which is due to the inherent smoothing in LADCP processing and the fact that ADCP measures an average velocity over the specified bin length, which was 16 m for the data used here. The results of both linear regressions exhibited an offset of $+0.4 \text{ cm s}^{-1}$, implying a NBADCP bias in both velocity components. No statistically significant dependence of the offset to temperature, pressure or backscatter strength could be found. Possible explanations of this bias is a displaced acoustic signal frequency or a dislocated Janus configuration. Velocity data from the BBADCP was not considered in the comparison.

A comparison between the LADCP and Pegasus data also was performed from the full-depth averaged velocity profiles. Here, barotropic tidal currents (see Appendix B) were removed to account for the different sampling times. Differences of the depths-averaged velocities showed a standard deviation of only 0.81 cm s^{-1} . The good quality of the depth-averaged LADCP data has

Table 2
Summary of the velocity comparisons

| Comparison | n | $\sigma(\Delta u)$ (cm s^{-1}) | $\sigma(\Delta v)$ (cm s^{-1}) | $\Delta \bar{u}$ (cm s^{-1}) | $\Delta \bar{v}$ (cm s^{-1}) | Least square fit |
|-------------------------------------|------|--|--|--|--|-------------------------------|
| $U_{\text{PEG}} - U_{\text{RCM}}$ | 18 | 1.57 | 1.30 | -0.16 ± 0.37 | 0.19 ± 0.31 | — |
| $U_{\text{RCM}} - U_{\text{LADCP}}$ | 29 | 4.32 | 4.84 | 0.49 ± 0.84 | 0.59 ± 0.94 | $0.14 U_{\text{RCM}} + 0.4$ |
| $U_{\text{PEG}} - U_{\text{LADCP}}$ | 5841 | 4.62 | 4.64 | 0.42 ± 0.06 | 0.37 ± 0.06 | $0.11 U_{\text{PEG}} + 0.4^a$ |

^a n is the number of compared values, $\sigma(\Delta U)$ the standard deviation of velocity differences, $\Delta \bar{U}$ the average velocity difference.

been discussed by Fischer and Visbeck (1993) and Firing (1998). In Section 3.2, these measurements are used to reference geostrophic currents. However, due to the large uncertainties in baroclinic LADCP velocities, we refrain from a description of the abyssal circulation on their basis.

Appendix B

Vertically averaged LADCP velocities contain current components that are not accounted for in the geostrophic approximation. The appendix briefly describes the treatment used in this study to remove those current components and provides an error estimate.

Before the vertically averaged LADCP (\bar{v}_{LADCP}) data were used to reference geostrophic velocities (v_{ref}), three velocity components of the LADCP were estimated and removed. Those were the barotropic tidal currents (v_{tide}), the ageostrophic current components (v_{ageo}) as Ekman, inertial and cyclostrophic currents and a velocity bias (v_{bias}), determined in Appendix A.

$$v_{\text{ref}} = \bar{v}_{\text{LADCP}} - v_{\text{tide}} - v_{\text{ageo}} - v_{\text{bias}} \quad (\text{B.1})$$

To avoid a degradation of the velocity measurements by barotropic tidal currents, the harmonic

constants of 15 tidal constituents were calculated from each mooring. In a first step, five major tidal constituents were calculated by harmonic analysis for each time series using 29 day segments. The results were used to infer 10 minor constituents on the basis of the tidal potential. To determine the barotropic tidal flow, the Fourier coefficients were finally projected on the barotropic and first three baroclinic vertical modes. The results for the M_2 and the K_1 are shown in Fig. 17. M_2 major axis amplitude is less than 2 cm s^{-1} in the central Somali Basin. However, strong barotropic tidal currents with amplitudes of more than 13 cm s^{-1} are present in the Socotra Passage.

Due to the use of 29-day segments, 16 individual determinations for each tidal constituent at each time series were to be obtained, allowing an error estimate. On average, the M_2 constituent tidal currents showed a mean standard deviation of 0.23 cm s^{-1} for the zonal and 0.28 cm s^{-1} for the meridional velocity, implying a standard error of less than 0.1 cm s^{-1} for each determination. The standard deviation of phase estimates was also small, less than 10° . However, tidal constituents with velocities smaller than 0.2 cm s^{-1} , e.g., the O_1 constituent, could not be resolved properly, because of large standard deviation of phase. Here, this velocity is taken as the error in the tidal velocity estimates.

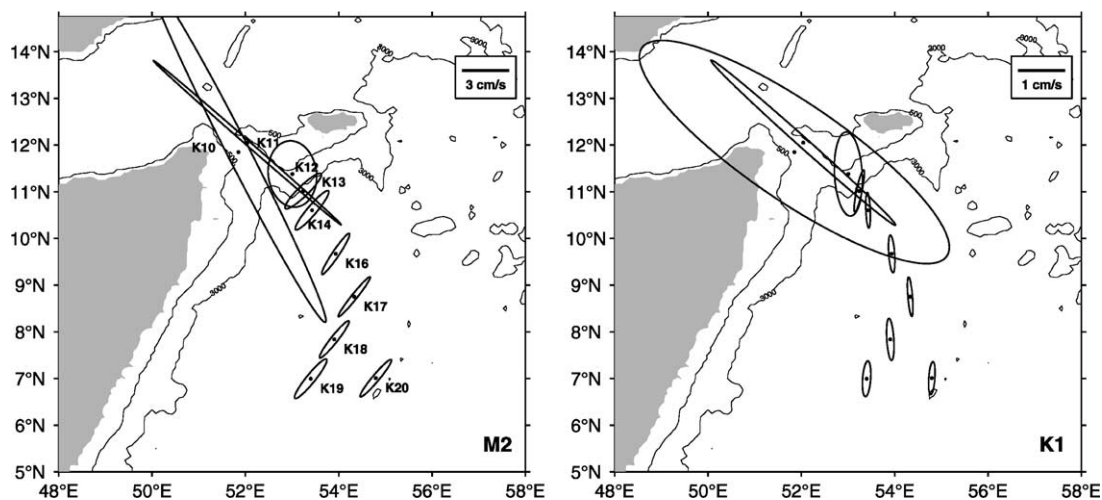


Fig. 17. Tidal currents of the M_2 constituent (left) and K_1 constituent (right).

The contributions of (v_{ageo}) were estimated for the upper water column, where they are presumed to be largest, only. Except for Ekman and inertial currents, cyclostrophic current contributions are particularly large within the Great Whirl (Fischer et al., 1996). For the determination of the ageostrophic current component, the difference between cross-track ADCP velocities, averaged between two CTD stations and the geostrophic velocities were used. Following Fischer et al. (1996), only the baroclinic flow field was taken into account. Both velocity shears were referenced at 350 m depths. Particularly large ageostrophic components were determined during the August cruise, where the SW-monsoon and the Great Whirl were fully developed. Here, an absolute section average of 30 cm s^{-1} was calculated for the depth range between 50 and 100 m. However, due to the fact that large ageostrophic velocities are limited to a small depth interval in the upper water column, their contributions to the depth-average velocities are small. The error in determining the ageostrophic contribution is estimated on the basis of the error of the ADCP velocity data, which was determined to be about 3 cm s^{-1} when averaged between stations. The overall contribution to the error for reference velocity was 0.15 cm s^{-1} for station depths larger 3500 m.

The largest error contribution to reference velocity originates from the inaccuracy of the measurement of depth-average velocity by the LADCP. Except for the LADCP bias, two major error sources are the inaccuracy of GPS position fixes and data gaps in the sampling due to bottom interference (e.g., Firing, 1998). Due to a duration of the LADCP casts of about 4 h, the root mean square uncertainty of GPS position fixes leads to an uncertainty in the depth averaged LADCP velocities of 0.6 cm s^{-1} . On average, 23 of the 8 s ensembles averages were unreliable due to bottom interference, which adds an additional uncertainty of 0.2 cm s^{-1} when assuming a rosette velocity of 10 cm s^{-1} . A possible LADCP compass error was investigated by comparing the LADCP velocity components with the Pegasus measurements, but no significant deviation was found.

In summary, the different error contributions to the reference velocity lead to a total root mean

square error of 1.2 cm s^{-1} , which is predominately due to GPS inaccuracy. Other error sources not included in this estimate, e.g., errors due to the limited horizontal resolution of the LADCP measurements or ocean interior ageostrophic motion are believed to be small for the area of interest. In fact as is shown in Section 3.2.3 the estimated reference velocity error is somewhat larger as suggested by the geostrophic transport calculations.

References

- Barton, E.D., Hill, A.E., 1989. Abyssal flow through the Amirante Trench (western Indian Ocean). *Deep-Sea Research* 36, 1121–1126.
- Beal, L.M., Molinari, R.L., Robbins, P.E., Chereskin, T.K., 2000. Reversing bottom circulation in the Somali Basin. *Geophysical Research Letters* 27, 2565–2568.
- Brandt, P., Stramma, L., Schott, F., Fischer, J., Dengler, M., Quadfasel, D., 2002. Annual Rossby waves in the Arabian Sea from TOPEX/POSEIDON altimeter and in situ data. *Deep-Sea Research II* 49, 1197–1210.
- Dengler, M., Quadfasel, D., 2002. Equatorial deep jets and abyssal mixing in the Indian Ocean. *Journal of Physical Oceanography*, in press.
- Eigenheer, A., 1997. Über den Einfluß von niederfrequenten Wellen auf die Monsunzirkulation im Indischen Ozean. Ph.D. Thesis, FB Geowissenschaften der Universität Hamburg, 106 Seiten.
- Fioux, M., Schott, F., Swallow, J.C., 1986. Deep boundary currents in the western Indian Ocean revisited. *Deep-Sea Research* 33, 415–426.
- Fioux, M., Swallow, J.C., 1988. Flow of deep water into the Somali Basin. *Deep-Sea Research* 35, 303–309.
- Firing, E., 1991. Acoustic Doppler current profiling measurements and navigation. Tech. rep., WHOI Publication 91-1, WOCE Report 68/91.
- Firing, E., 1998. Lowered ADCP development and use in WOCE. Intern. WOCE Newsletter 30, 10–14.
- Fischer, J., Schott, F., Stramma, L., 1996. Currents and transports of the Great Whirl-Socotra Gyre system during the summer monsoon August 1993. *Journal of Geophysical Research* 101 (C2), 3573–3587.
- Fischer, J., Visbeck, M., 1993. Deep velocity profiling with self-contained ADCPs. *Journal of Atmospheric and Oceanic Technology* 10, 764–773.
- Fischer, R.L., Jantsch, M.Z., Comer, R.L., 1982. General bathymetric chart of the oceans (GEPCO), map 5.09. Canadian Hydrographic Service, Ottawa.
- Johnson, D.A., Damuth, J.E., 1979. Deep thermohaline flow and current-controlled sedimentation in the Amirante Passage: Western Indian Ocean. *Marine Geology* 33, 1–44.

- Johnson, G.C., Musgrave, D.L., Warren, B.A., Field, A., Olson, D.B., 1998. Flow of bottom and deep water in the Amirante Passage and Mascarene Basin. *Journal of Geophysical Research* 103, 30973–30984.
- Johnson, G.C., Warren, B.A., Olson, D.B., 1991a. Flow of bottom water in the Somali Basin. *Deep-Sea Research* 38, 637–652.
- Johnson, G.C., Warren, B.A., Olson, D.B., 1991b. A deep boundary current in the Arabian Sea. *Deep-Sea Research* 38, 653–661.
- Joyce, T., Corry, C., 1991. Requirements for WOCE hydrographic programme data reporting. Tech. rep., WHPO Publication 90-1, Rev. 2, WOCE Report 67/91. 144pp.
- Liu, Z., Wu, L., Bayler, E., 1999. Rossby wave-coastal Kelvin wave interaction in the extratropics. Part I: Low-frequency adjustment in a closed basin. *Journal of Physical Oceanography* 29, 2382–2404.
- Luyten, J.R., 1982. Equatorial current measurements, I. moored observations. *Journal of Marine Research* 40, 19–41.
- Quadfasel, D., Fischer, J., Schott, F., Stramma, L., 1997. Deep water exchange through the Owens Fracture Zone in the Arabian Sea. *Geophysical Research Letters* 24, 2805–2808.
- Sanford, T.B., 1991. Spatial structures of thermocline and abyssal waves. In: Müller, P., Henderson, D. (Eds.), *Dynamics of Oceanic Internal Gravity Waves*. 'Aha Huliko'a Hawaiian Winter Workshop. University of Hawaii at Manoa, pp. 109–142.
- Schott, F., Fischer, J., 2000. Winter monsoon circulation of the northern Arabian Sea and Somali Current. *Journal of Geophysical Research* 105, 6359–6376.
- Schott, F., Fischer, J., Gartnericht, U., Quadfasel, D., 1997. Summer monsoon response of the northern Somali Current, 1995. *Geophysical Research Letters* 24, 2565–2568.
- Schott, F., Pollehne, F., Quadfasel, D., Stramma, L., Wiesner, M., Zeitzschel, B., 1996. Arabian Sea 1995. Cruise No. 32, 23 March–19 December 1995. *Meteor Berichte* 95-6, 163 pp.
- Schott, F., Swallow, J.C., Fieux, M., 1989. Deep currents underneath the equatorial Somali Current. *Deep-Sea Research* 36 (8), 1191–1199.
- Send, U., 1994. Accuracy of velocity profile measurements: Effect of tropical and midlatitude internal waves. *Journal of Geophysical Research* 99 (C8), 16229–16236.
- Send, U., Visbeck, M., Krahnmann, G., 1996. Aspects of acoustic transponder surveys and acoustic navigation. *IEEE Oceans* 96, 1631–1642.
- Sengupta, D., Senan, R., Goswami, B.N., 2001. Origin of intraseasonal variability of circulation in the tropical central Indian Ocean. *Geophysical Research Letters* 28, 1267–1270.
- Sloyan, B.M., Rintoul, S.R., 2001. The Southern Ocean limb of the global deep overturning circulation. *Journal of Physical Oceanography* 31, 143–173.
- Smith, W.H.F., Sandwell, D.T., 1997. Global sea floor topography from satellite altimetry and ship depth soundings. *Science* 2775, 1956–1962.
- Spain, P.F., Dorson, D.L., Rossby, H., 1981. Pegasus: A simple, acoustically tracked velocity profiler. *Deep-Sea Research* 28, 1553–1567.
- Spencer, D., Broecker, W.S., Craig, H., Weiss, R.F., 1982. Sections and profiles. In: *GEOSECS Indian Ocean Expedition*, Vol. 6, National Science Foundation, Washington, DC, 140 pp.
- Stommel, H., Arons, A.B., 1960. On the abyssal circulation of the world ocean-I. Stationary planetary flow patterns on a sphere. *Deep-Sea Research* 6, 140–154.
- Toole, J.M., Warren, B.A., 1993. A hydrographic section across the subtropical south Indian Ocean. *Deep-Sea Research I* 40, 1973–2019.
- Warren, B.A., 1978. Bottom water transport through the Southwest Indian Ridge. *Deep-Sea Research* 13, 315–321.
- Warren, B.A., 1981a. Deep circulation to the World Ocean. In: Warren, B.A., Wunsch, C. (Eds.), *Evolution of Physical Oceanography*. The MIT Press, Cambridge, MA, pp. 6–41.
- Warren, B.A., 1981b. Transindian hydrographic section at Lat. 18°S: Property distributions and circulation in the South Indian Ocean. *Deep-Sea Research* 28, 759–788.
- Warren, B.A., 1993. Circulation of north Indian deep water in the Arabian Sea. In: Desai, B.N. (Ed.), *Oceanography in the Indian Ocean*. A.A. Balkema, Rotterdam, pp. 575–582.
- Warren, B.A., Johnson, G.C., 1992. Deep currents in the Arabian Sea. *Marine Geology* 104, 279–288.
- Warren, B.A., Johnson, G.C., 2002. The overflows across the Ninetyeast Ridge. *Deep-Sea Research II* 49, 1423–1439.
- Warren, B.A., Stommel, H., Swallow, J.C., 1966. Water masses and patterns of flow in the Somali Basin during the southwest monsoon of 1964. *Deep-Sea Research* 13, 825–860.
- Wirth, A., Willebrand, J., Schott, F., 2002. Variability of the Great-Whirl from observations and models. *Deep-Sea Research II* 49, 1279–1295.
- Wunsch, C., 1996. *The Ocean Circulation Inverse Problem*. Cambridge University Press, Cambridge 422pp.
- Wyrtki, K., 1971. *Oceanic Atlas of the International Indian Ocean Expedition*. National Science Foundation Washington, DC 531 pp.
- Zhang, H.M., Talley, L.D., 1998. Heat and buoyancy budgets and mixing rates in the upper thermocline of the Indian and global Oceans. *Journal of Physical Oceanography* 28, 1961–1978.